Molecular Crystals and Liquid Crystals
Publication details, including instructions for authors and subscription information:
http://www.tandfonline.com/loi/gmcl16

Photoinduced Absorption and Resonant Raman Scattering in Trans-$(CD)_x$

Z. Vardeny [a], O. Brafman [a] & E. Ehrenfreund [a]
[a] Department of Physics and Solid State Institute, Technion, Haifa, 32000, Israel
Version of record first published: 17 Oct 2011.

To cite this article: Z. Vardeny , O. Brafman & E. Ehrenfreund (1985): Photoinduced Absorption and Resonant Raman Scattering in Trans-$(CD)_x$, Molecular Crystals and Liquid Crystals, 117:1, 355-362

To link to this article: http://dx.doi.org/10.1080/00268948508074651

Mol. Cryst. Liq. Cryst. 1985, Vol. 117, pp. 355-362
0026-8941/85/1174-0355/$15.00/0

Printed in the United States of America

PHOTOINDUCED ABSORPTION AND RESONANT RAMAN SCATTERING IN TRANS-$(CD)_x$

Z. VARDENY, O. BRAFMAN AND E.EHRENFREUND
Department of Physics and Solid State Institute, Technion, Haifa 32000, Israel

Abstract The three resonantly enhanced Raman modes and the three photoinduced ir-active vibrations in trans-$(CD)_x$ are described in terms of amplitude modes of the Peierls gap and charged induced ir-active modes, respectively. The detailed spectra are accounted for by a dressed phonon propagator and a coupling parameter. The photoinduced electronic bands and the primary Raman frequencies increase with increasing temperature; the origin of this anomaly is discussed.

INTRODUCTION

It is now well established[1] that trans-polyacetylene undergoes a spontaneous symmetry breaking dimerization due to the Peierls instability, which causes an energy gap $2\Delta_o$ in its π electronic system. Δ_o is primarily determined by the electron-phonon (e-p) interaction; the same e-p interaction causes a renormalization of the strongest coupled phonons[2]. The electronic gap and the strongly coupled phonons are therefore intimately related and it is possible to analyze the electronic system in polyacetylene by investigating the phonon spectrum. Perhaps the best techniques suitable for showing the relation between the phonons and the electronic gap are resonant Raman scattering (RRS) and photoinduced absorption (PA).

The RRS spectra in trans-polyacetylene show two kinds of Raman lines[3]. Three primary lines, which do not shift with the excitation laser frequency ω_L, and satellite lines which shift to higher frequencies with ω_L (dispersion). This dispersion is explained[2] by the existence of disorder in the films which causes a distribution $P(\Delta)$ in the gap Δ, and consequently different phonons are resonantly enhanced when ω_L is varied. The PA spectrum in trans-polyacetylene is due to vibrations[4] and electronic bands[5]. Below 0.2 eV, 3 sharp ir-active vibrations (IRAV) were discovered[6]; their frequencies are isotope dependent[6,7]. Two main electronic PA bands were also discovered[5]. The lower energy band ($\simeq$ 0.45 eV) is due to localized charge defects; the higher energy band ($\simeq$ 1.4 eV) is

due to neutral excitations. A successful approach was recently developed[2] which could explain all details of RRS and induced IRAV spectra, based on the amplitude mode (AM) formalism[8].

In this work we present PA and RRS measurements done simultaneously on the same films of trans-$(CD)_x$. We show that the 3 IRAV can be directly connected with the 3 RRS phonons using the AM formalism. We also report an unusual temperature dependence of the electronic PA energies and the primary RRS frequencies; they increase with increasing temperature. This behaviour is in accord with the Peierls type gap in trans-polyacetylene and also confirms the AM identification for the RRS vibrations.

RESONANT RAMAN SCATTERING IN TRANS-$(CD)_x$

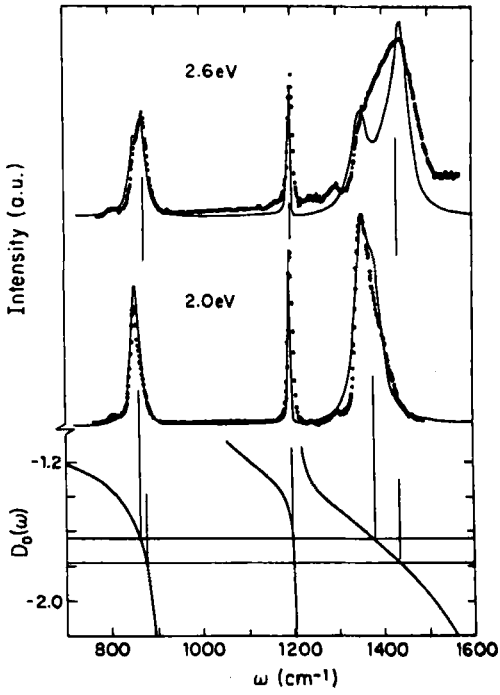

Fig. 1: RRS spectra of trans-$(CD)_x$ at 300K; $\hbar\omega_L$ are indicated. The dots are experimental, full lines are theoretical fit[2]. $D_o(\omega)$ is displayed and the horizontal lines correspond to the two resonance conditions.

The trans-$(CD)_x$ sample was polymerized at Nagoya University in the form of a thin film (thickness of about 0.2 μm) grown on KBr substrate; the film was isomerized by heat treatment at 180°C for 10 minutes. Typical RRS spectra at 300K excited with $\hbar\omega_L$ = 2 eV and 2.6 eV are shown in Fig. 1. The primary frequencies at 300K are: ω_1^R = 855, ω_2^R = 1198 and ω_3^R = 1362 cm^{-1}.

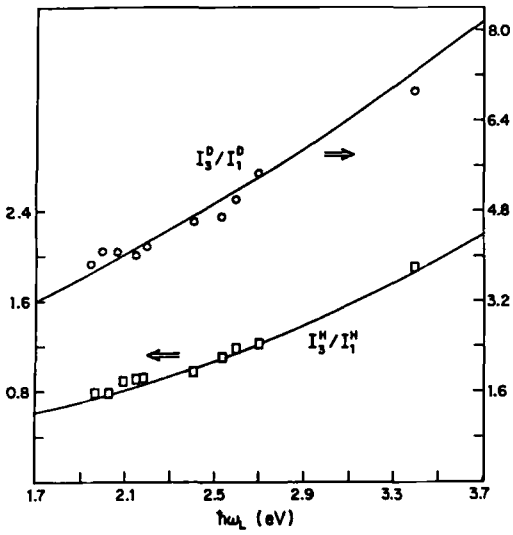

Fig. 2: The RRS integrated intensity I_3^R/I_1^R vs. ω_L. Circles - $(CD)_x$, squares - $(CH)_x$. The full lines are calculated based on the $D_o(\omega)$ functions of these isotopes.

The integrated intensity ratios at $\hbar\omega_L = 2$ eV are $I_3^R/I_1^R \simeq 3.8$ and $I_3^R/I_2^R \simeq 6$. Both I_3^R/I_1^R and I_3^R/I_2^R ratios increase with ω_L, as shown in Fig. 2 for I_3^R/I_1^R. We note that the I_3^R/I_1^R ratio increase also in trans-$(CH)_x$, as shown in Fig. 2. The satellite dispersion $\delta\omega(\omega_L)$ is the largest for mode 3 in $(CD)_x$ (Fig. 1). All these properties are well accounted for by the AM approach[8].

The dressed phonon frequencies ω_n^R are given in the AM formalism by[2,8]

$$D_o(\omega) = \sum_{n=1}^{3} \frac{\lambda_n}{\lambda} \frac{(\omega_n^o)^2}{\omega^2 - (\omega_n^o)^2} = \frac{-1}{1 - 2\tilde{\lambda}} \qquad (1)$$

where ω_n^o are the three bare-phonon frequencies and λ_n are their corresponding dimensionless e-p couplings. In Eq. (1) $\lambda = \Sigma\lambda_n$ and $1-2\tilde{\lambda} = 2\,E_i''(\Delta_o)$, where $E_i(\Delta)$ is the condensation energy and $2\Delta_o$ is the dimerization gap. For a Peierls system[2,8]

$$2\Delta_o = 4E_c \exp(-1/2\lambda) \qquad (2)$$

$\tilde{\lambda} = \lambda$ and E_c is a cut-off energy.

The cross-section σ_R for RRS from AM has the form[2]

$$\sigma_R \sim |f(\omega_L/2\Delta_o)|^2 \, \mathrm{Im} \frac{D_o(\omega)}{1 + (1-2\tilde{\lambda})D_o(\omega)} \qquad (3)$$

where $D_o(\omega)$ is defined in Eq. (1) and $|f|^2$ is strongly peaked[9]

at $\hbar\omega_L = 2\Delta_o$. The poles of Eq. (3) gives ω_n^R (Eq. 1) while the line integrated intensity I_n^R (and line-width) is proportional to the residue at each pole[2], i.e. to the inverse of $D_o'(\omega) \equiv \partial D_o(\omega)/\partial\omega$ at $\omega = \omega_n^R$. $D_o(\omega)$ contains therefore the entire information about the frequencies, the relative intensities and the relative widths of the RRS lines.

The function $D_o(\omega)$ for $(CD)_x$ shown in Fig. 1 was obtained previously[2] by fitting the 3 satellite frequencies at various ω_L. $D_o(\omega)$ parameters are: $\omega_1^o = 921$, $\lambda_1/\lambda = 0.06$, $\omega_2^o = 1207$, $\lambda_2/\lambda = 0.01$, $\omega_3^o = 2040$, $\lambda_3/\lambda = 0.93$. We note that ω_3 has the strongest e-p coupling and it is not surprising that the shift from its bare frequency ω_3^o is the largest. Fig. 1 shows how ω_n^R increase with ω_L. At higher ω_L resonance conditions are matched by larger $2\Delta_o$ (and from Eq. (2) also larger λ) so that the horizontal lines drawn at $-1/(1-2\lambda)$ intersect $D_o(\omega)$ at higher frequencies. Using the product rule for AM frequencies[8]

$$(\omega_n^R/\omega_n^o)^2 = 2\tilde{\lambda} \qquad (4)$$

We showed[2] that the Peierls gap equation (Eq. (2)) holds for polyacetylene, with $E_c = 6.3$ eV. The two horizontal lines for the two ω_L were calculated using Eq. (2). The theoretical fit shown in Fig. 1 was calculated[2] assuming a narrow distribution in the parameter λ. With no additional adjustable parameter we calculate in Fig. 2 the dependence of I_3^R/I_1^R on ω_L using $D_o(\omega)$ and Eq. (2); the agreement with the experimental values is remarkably good.

PHOTOINDUCED IRAV IN TRANS-$(CD)_x$

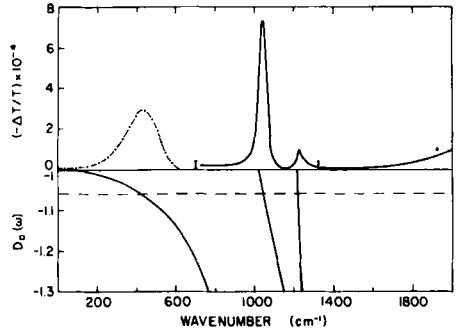

Fig. 3: Photoinduced IRAV in trans-$(CD)_x$. The dashed line is theoretical[7]. $D_o(\omega)$ is displayed and the horizontal line intersections give the IRAV frequencies.

The same $(CD)_x$ film was used for PA measurements. The experimental set-up for steady-state PA is described elsewhere[7]. In Fig. 3 the induced absorption $(-\Delta T/T)$ at 80K obtained with a

laser intensity of 20 mW cm^{-2} is plotted vs. the probe energy up to 2000 cm^{-1}. Two IRAV modes are photoinduced at ω_2^i = 1045 and ω_3^i = 1225 cm^{-1}. Blanchet et al.[6] have extended the PA measurements to lower energies and reported in $(CD)_x$ a third mode at $\omega_1^i \simeq 400$ cm^{-1}; this mode is also shown (schematically) in Fig. 3. There are therefore a total of 3 IRAV in $(CD)_x$, as in the RRS spectrum. However, there exist several differences between PA (Fig. 3) and the RRS (Fig. 1) spectra. (i) $\omega_n^i < \omega_n^R$ for all three modes. (ii) The integrated intensity I_n^i of the 3 IRAV modes are very different from the respective intensities in RRS. (iii) We have not noticed any changes in the IRAV spectrum with ω_L. However, a distinct connection exists between the IRAV and the RRS vibrations as revealed by the AM theory[2]: the IRAV can be derived by the same $D_o(\omega)$ function using the same form of the dressed phonon propagator as in RRS.

When charges are added to the chain $\Delta\alpha$ is given by[8]

$$\Delta\alpha(\omega) \sim \frac{\omega D_o(\omega)}{1 + (1-\alpha_p) D_o(\omega)} \qquad (5)$$

where $D_o(\omega)$ is defined in Eq. (1) and α_p is a pinning parameter. The IRAV are the poles of Eq. (5) and their frequencies ω_n^i satisfy the equation $D_o(\omega) = -1/(1-\alpha_p)$. Similarly as for the RRS case[7], the integrated IRAV intensities I_n^i are proportional to $\omega_n^i / D'(\omega_n^i)$. A similar product rule as for RRS (Eq. (4)) exists also for the IRAV[8], namely $(\omega_n^i/\omega_n^o)^2 = \alpha_p$.

$D_o(\omega)$ inferred from RRS is plotted in Fig. 3 and its intersections with the horizontal line drawn at $-1/(1-\alpha_p)$ with $\alpha_p \simeq 0.055$, inferred from the IRAV product rule, accurately give the three experimental IRAV frequencies[7]. This process yields the correct IRAV relative intensities. With α_p value found above we calculate $I_3^i/I_2^i = 0.09$ while the experimental value is 0.07. We conclude therefore that all IRAV phonons induced by photogeneration (or by doping) are determined by the Raman data and a pinning parameter.

TEMPERATURE DEPENDENCE

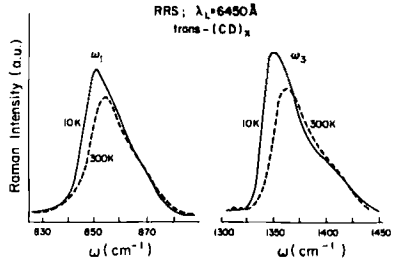

Fig. 4: RRS spectrum of ω_1 and ω_3 in $(CD)_x$ at 10 and 300K.

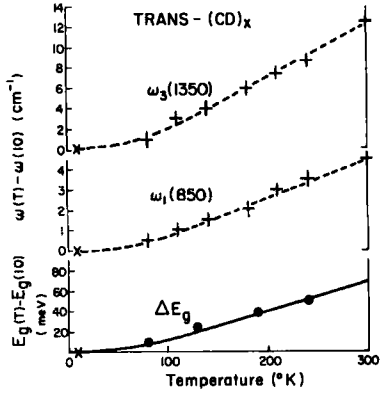

Fig. 5: The shift $\omega(T) - \omega(10)$ of the primary peak positions for ω_1 and ω_3 in $(CD)_x$. ΔE_g is the shift of the electronic PA bands. The lines are drawn to guide the eyes.

We measured RRS and PA as a function of temperature. The two Raman lines ω_1^R and ω_3^R are shown in Fig. 4 at 10 and 300K. The primary frequencies increase with increasing temperature and Fig. 5 shows the shift $\Delta\omega(T) = \omega(T) - \omega(10)$ for both modes. $\Delta\omega_3(T)$ is larger than $\Delta\omega_1(T)$ and it reaches ~ 13 cm^{-1} at 300K. We also found upward shifts for ω_1 and ω_3 in trans-$(CH)_x$, however for this isotope $\Delta\omega_1(T) \simeq \Delta\omega_3(T)$.

Normal phonon frequencies decrease when the temperature increases, due to the force constants softening at high temperature. We found that the weakest coupled phonon in $(CD)_x$ (ω_2) has the regular temperature dependence: ω_2 decreases by 4 cm^{-1} from 10K to 300K. This shows that the unusual upward shift for ω_1 and ω_3 is caused by their stronger e-p couplings whose temperature dependence overcomes the force-constants softening. This confirms that the phonons in trans-polyacetylene are renormalized and the e-p interaction must be included in any lattice dynamics calculation[10]. From the AM product rule (Eq. (4)) we can conclude that the increase in the phonon frequencies reflects an increase in the e-p coupling . This is shown schematically in Fig. 6 where the two horizontal lines are drawn at $-(1-2\lambda)^{-1}$ at 80 and 300K and λ increases with temperature. Changes in λ influence ω_3 much more than ω_1, since $[D'(\omega_3)]^{-1} > [D'(\omega_1)]^{-1}$ (Fig. 6) for the values of $D_o(\omega)$ suitable for RRS. This explains why $\Delta\omega_3(T) > \Delta\omega_1(T)$. We note that for the satellite dispersion $\delta\omega(\omega_L)$ we also found $\delta\omega_3 > \delta\omega_1$. This is caused by the same mechanism as for the temperature shift; λ increases with ω_L and $(D_3')^{-1} > (D_1')^{-1}$. The opposite temperature shift $\Delta\omega_2 < 0$ for ω_2 in $(CD)_x$ cannot be explained by Fig. 6 since $D_o(\omega)$ does not contain yet the changes expected in ω_n^o with temperature (ω_n^o should decrease with temperature like regular phonons).

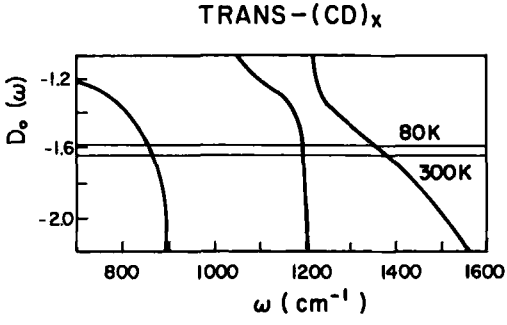

Fig. 6: $D_o(\omega)$ of trans-$(CD)_x$[2]. The two horizontal line intersections give ω_1 and ω_3 primary frequencies at 80 and 300K.

We measured an upward shift with increasing temperature for all electronic PA bands. This include the low-energy band, the high-energy band and also the oscillations found in PA[5] in the energy range of 1.4 to 1.7 eV. The average shift ΔE_g of the oscillations in the PA spectrum as a function of temperature, is shown in Fig. 5. An upward shift was reported[6] also for the doping-induced "mid-gap" absorption. Finally, similar upward shifts were reported for the ir photoluminescence in trans-polyacetylene[11].

Since all these various energies are associated with Δ_o, their upward shift indicate that the energy-gap itself increases with temperature. This is in contrast to the behaviour of conventional semiconductors[12] with direct-gap (GaAs) or indirect gap (Ge, Si). In all of them the optical gap decreases with temperature. The Peierls gap-equation (Eq. (2)) may explain this anomaly. We have concluded from RRS that λ increases with the temperature and Eq. (2) yields higher Δ_o for larger λ. A detailed calculation of Δ_o shift with temperature based on the RRS results, will be published elsewhere[13].

ACKNOWLEDGEMENTS

We thank Professor J. Tanaka for providing us the $(CD)_x$ sample and F. Coter for technical help. This work was supported in part by the Israel Academy for Basic Research, Jerusalem, Israel.

REFERENCES

1. Proc. Int. Conf. on the Physics and Chemistry of Conducting Polymers; Les-Arcs, France. Jour. de Physique C3, 44 (1983).

2. Z. Vardeny, E. Ehrenfreund, O. Brafman and B. Horovitz, Phys. Rev. Lett. 51, 2326 (1983).
3. D. B. Fitchen, Mol. Cryst. Liq. Cryst. 83, 1127 (1982).
4. Z. Vardeny, J. Orenstein and G. L. Baker, Phys. Rev. Lett. 50, 2032 (1983).
5. J. Orenstein, G. Baker and Z. Vardeny, in Ref. 1, p. 407.
6. G. B. Blanchet, C. R. Fincher, T. C. Chung and A. J. Heeger, Phys. Rev. Lett. 50, 1938 (1983).
7. Z. Vardeny, J. Tanaka, H. Fujimoto and M. Tanaka, Sol. State Commun. 50, 937 (1984).
8. B. Horovitz, Sol. State Commun. 41, 729 (1982).
9. B. Horovitz, Z. Vardeny, E. Ehrenfreund and O. Brafman, Synthetic Metals 9, 215 (1984).
10. E. J. Mele and M. J. Rice, Sol. State Commun. 34, 339 (1980).
11. K. Yoshino, S. Hayashi, Y. Inuischi, K. Hattori and Y. Watanabe, Sol. State Commun. 46, 583 (1983).
12. G. D. Cody in Hydrogenated Amorphous Silicon, ed. J. Pankove (Academic Press, 1984), Chap. 2, Vol. 21B, and references therein.
13. Z. Vardeny, O. Brafman and E. Ehrenfreund, to be published.